International Journal of
Molecular Sciences

MDPI

Article

Na^+ Translocation Dominates over H^+-Translocation in the Membrane Pyrophosphatase with Dual Transport Specificity

Alexander V. Bogachev [1], Viktor A. Anashkin [1], Yulia V. Bertsova [1], Elena G. Zavyalova [2] and Alexander A. Baykov [1,*]

[1] Belozersky Institute of Physico-Chemical Biology, Lomonosov Moscow State University, Moscow 119899, Russia; bogachev@belozersky.msu.ru (A.V.B.); victor_anashkin@belozersky.msu.ru (V.A.A.)
[2] Department of Chemistry, Lomonosov Moscow State University, Moscow 119899, Russia; zlenka2006@gmail.com
* Correspondence: baykov@belozersky.msu.ru

Abstract: Cation-pumping membrane pyrophosphatases (mPPases; EC 7.1.3.1) vary in their transport specificity from obligatory H^+ transporters found in all kingdoms of life, to Na^+/H^+-co-transporters found in many prokaryotes. The available data suggest a unique "direct-coupling" mechanism of H^+ transport, in which the transported proton is generated from nucleophilic water molecule. Na^+ transport is best rationalized by assuming that the water-borne proton propels a prebound Na^+ ion through the ion conductance channel ("billiard" mechanism). However, the "billiard" mechanism, in its simple form, is not applicable to the mPPases that simultaneously transport Na^+ and H^+ without evident competition between the cations (Na^+,H^+-PPases). In this study, we used a pyranine-based fluorescent assay to explore the relationship between the cation transport reactions catalyzed by recombinant *Bacteroides vulgatus* Na^+,H^+-PPase in membrane vesicles. Under appropriately chosen conditions, including the addition of an H^+ ionophore to convert Na^+ influx into equivalent H^+ efflux, the pyranine signal measures either H^+ or Na^+ translocation. Using a stopped-flow version of this assay, we demonstrate that H^+ and Na^+ are transported by Na^+,H^+-PPase in a ratio of approximately 1:8, which is independent of Na^+ concentration. These findings were rationalized using an "extended billiard" model, whose most likely variant predicts the kinetic limitation of Na^+ delivery to the pump-loading site.

Keywords: energy coupling; direct coupling; proton pump; Na^+ pump; billiard mechanism; pyranine; ETH 157; transport assay; stopped flow

Citation: Bogachev, A.V.; Anashkin, V.A.; Bertsova, Y.V.; Zavyalova, E.G.; Baykov, A.A. Na^+ Translocation Dominates over H^+-Translocation in the Membrane Pyrophosphatase with Dual Transport Specificity. *Int. J. Mol. Sci.* **2024**, *25*, 11963. https://doi.org/10.3390/ijms252211963

Academic Editor: Larry Fliegel

Received: 4 October 2024
Revised: 1 November 2024
Accepted: 5 November 2024
Published: 7 November 2024

1. Introduction

Integral membrane pyrophosphatase (mPPase; EC 7.1.3.1), initially found in photosynthetic bacteria [1,2] and later in plants, protists, and many prokaryotes, catalyzes the active transport of H^+ and/or Na^+ out of cytoplasm [3–9]. The transport reaction is fueled by pyrophosphate (PP_i), whose hydrolysis releases nearly as much energy as ATP hydrolysis (20–25 versus 35 kJ/mol) [10]. The transport function of mPPase establishes a link between chemiosmotic energy and the concentration of PP_i, the important regulator of numerous biosynthetic reactions that produce it as a by-product [10]. In some organisms, especially plants, the reverse reaction of PP_i synthesis at the expense of chemiosmotic energy may also be physiologically significant [11]. mPPase-containing organisms are generally resistant to various types of stress, and this property is further enhanced in engineered mutants with increased mPPase production [12–14].

mPPases are divided into three families according to their transport specificities [5]. H^+-PPases transport only protons, whereas Na^+-PPases transport only Na^+ at its physiological concentrations [15,16], but both Na^+ and H^+ at <5 mM Na^+ concentrations [17]. In other words, the H^+-transport activity of Na^+-PPases is inhibited at high Na^+ concentrations—their catalytic cycle is apparently associated with the transport of either a sodium ion or

a proton, but not both. This inhibition is weak or even absent in members of the third mPPase family (Na^+,H^+-PPases), which transport both cations even in the presence of 100 mM Na^+ [18,19]. All mPPases absolutely require Mg^{2+} for the transport and hydrolytic activities. K^+ is a positive modulator of both Na^+-transporting mPPase families and some members of the H^+-PPase family.

The three mPPase families have very similar structures that are unique to the protein world [20–22]. All mPPases are homodimers of approximately 70-kDa α-helical subunits. Each subunit forms a funnel-like structure with a hydrophilic cavity (hydrolytic center) in the cytoplasmic part. The cavity contains protein ligands for five Mg^{2+} ions and pyrophosphate and nucleophilic water molecules. A gated exit channel connects the hydrolytic center to the other side of the membrane (vacuolar lumen or periplasmic space). The major difference between Na^+-PPase and H^+-PPase is the channel position of the conserved Glu residue that forms a Na^+-binding site in the Na^+-PPase [23].

The structural similarity of the three mPPase subfamilies suggests a common coupling mechanism. H^+-PPase is structurally poised to "direct coupling", wherein the transported proton is generated by the nucleophilic water molecule during its attack on PP_i in the catalytic site (the "chemical" proton) and is translocated to the adjacent exit channel via short proton wires linking auxiliary proton-binding sites [20]. Direct coupling appears to be a cornerstone of the H^+ translocation mechanism in both H^+-PPase [3,20] and the two Na^+-transporting mPPase subfamilies when they function as H^+ transporters [3]. This H^+ transport mechanism provides a simple venue to the Na^+ transport via creating an intermediate Na^+-binding site on the proton path through the channel (Figure 1A). Such a site formed by the aforementioned Glu residue was indeed found in the crystal structure of Na^+-PPase [21]. In the "billiard" mechanism of the Na^+ transport [3], the water-borne proton electrostatically pushes the bound Na^+ ion through the exit channel. In the framework of this mechanism, the dual specificity of Na^+-PPase at low Na^+ concentrations is explained by the ability of the Na^+-binding site to competitively accommodate the Na^+ and proton (Figure 1B).

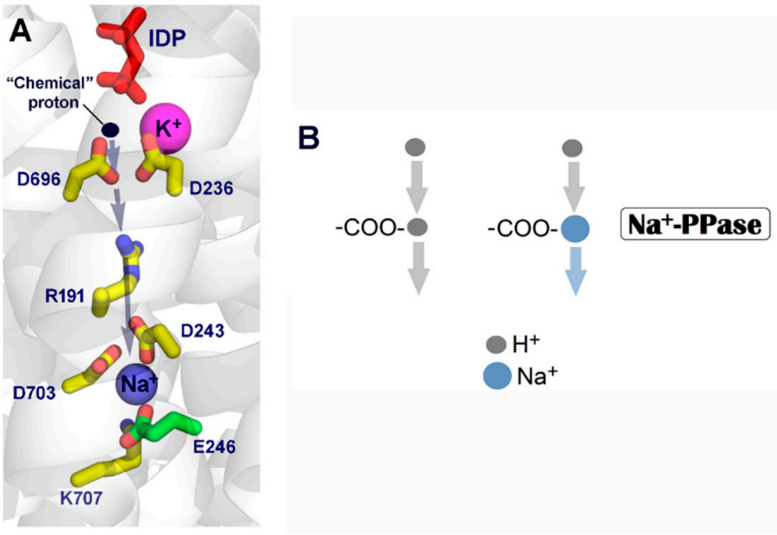

Figure 1. The "billiard" mechanism of Na^+ transport by mPPases. (**A**) Part of the ion conductance channel between the active site and ionic gate in *Thermotoga maritima* Na^+-PPase with bound substrate analog (imidodiphosphate), Na^+, and K^+ (PDB code: 5LZQ) [23]. All amino acid residues are shown in a one-letter notation. Asp residues 696 and 236 coordinate the nucleophilic water molecule, Glu246 is the Na^+ ligand, and the four other amino acid residues are parts of the exit channel. The arrows indicate the presumed path of the "chemical" proton in Na^+-PPase through the "proton wire" to the bound Na^+ ion; (**B**) Competition between H^+ and Na^+ in the transport reaction is determined by the relative affinities of the transitory site (Glu246 carboxylate) for the two cations. This figure was reproduced from Baykov et al. [3] under the terms of the Creative Commons CC BY license.

However, the "billiard" mechanism, in its simple form, cannot explain the transport specificity of the so-called Na^+,H^+-PPases that transport H^+ along with Na^+ even in the presence of 100 mM Na^+, suggesting that the two transport reactions are independent [18,19]. Two hypothetical explanations have been proposed—one assumes that both transport reactions occur in the same subunit [3], while the other posits that they occur in different subunits within a dimer [22]. Much uncertainty about the pumping mechanism of Na^+,H^+-PPase could be resolved by measuring the H^+/Na^+ pumping ratio/stoichiometry. However, this important parameter has remained unknown because previous transport assays of the two cations were based on different principles—$^{22}Na^+$ uptake and ΔpH indicator fluorescence change, not allowing quantitative comparisons.

We describe here an indirect pyranine-based assay that allows the separate monitoring and quantification of both transport reactions on a millisecond scale. By using the assay with homodimeric *Bacteroides vulgatus* Na^+,H^+-translocating mPPase (*Bv*-mPPase), we show that the Na^+/H^+ transport ratio is much less than unity under a variety of conditions. This finding rules out the simple competition model of Na^+ and H^+ transport via the same protein machinery and transport mechanism, suggesting a unique coupling mechanism for this relict ion pump.

2. Results

2.1. The Unified Procedure to Measure Na^+ and H^+ Transport into Membrane Vesicles

mPPase from *B. vulgatus* was the first characterized Na^+,H^+-PPase capable of simultaneous translocation of Na^+ and H^+ over a wide range of their concentrations in the medium [18]. Knowing the ratio of the Na^+ and H^+ transport rates is important for the diagnosis of Na^+,H^+-PPase mechanism. A ratio close to unity would indicate the asymmetrical functioning of transporter subunits, such that one subunit transports Na^+ and the other transports H^+, as proposed in a recent publication [22]. On the other hand, the prevalence of one activity would favor the transport promiscuity of both subunits.

Therefore, we developed a unified procedure for estimating the rates of concurrent Na^+ and H^+ transport into inverted membrane vesicles harboring *Bv*-mPPase in the membrane and pyranine in the lumen. This pH indicator fluoresces only in a deprotonated form, allowing one to monitor H^+ translocation through the vesicle membrane in both directions [24–26]. The advantage of pyranine as a pH indicator over the more common acridines is that it reports on changes in pH in the aqueous phase rather than ΔpH across the membrane and its response is therefore more linear. The pyranine response is bidirectional, less prone to artefact formation, and much more rapid because it does not require an indicator transport through the membrane.

The principle of the assay is illustrated in Figure 2. *Bv*-mPPase establishes fluxes of Na^+ and H^+ into vesicles produced from recombinant *E. coli* cells (Figure 2). If the Na^+ ionophore ETH 157 is present, it will return the Na^+ ions to the outer medium (blue arrow in Figure 2A). Furthermore, the Na^+ ionophore allows the translocation of additional Na^+ ions (red arrow in Figure 2A) to compensate for the charge coming with the translocated H^+ ions. This helps to avoid transport rate limitation by the transmembrane electric potential difference Δψ. The total rate of passive Na^+ transport by ETH 157 is equal to the sum of the rates of Na^+ and H^+ pumping by *Bv*-mPPase, resulting in *acidification* (H^+ accumulation) inside the vesicles. In the presence of ETH 157, the pyranine fluorescence reports thus on H^+ pumping into the vesicles with no interference from the Na^+ transport, which does not affect the vesicle acidity directly. According to the pyranine titration curve, a 10% change in the pyranine fluorescence will result from a pH change of approximately 0.2 unit. In a suspension of pyranine-loaded vesicles, the same pH change in the vesicle lumen is expected to cause a smaller relative change in the measured fluorescence because of the background signal from the contaminating pyranine in the medium.

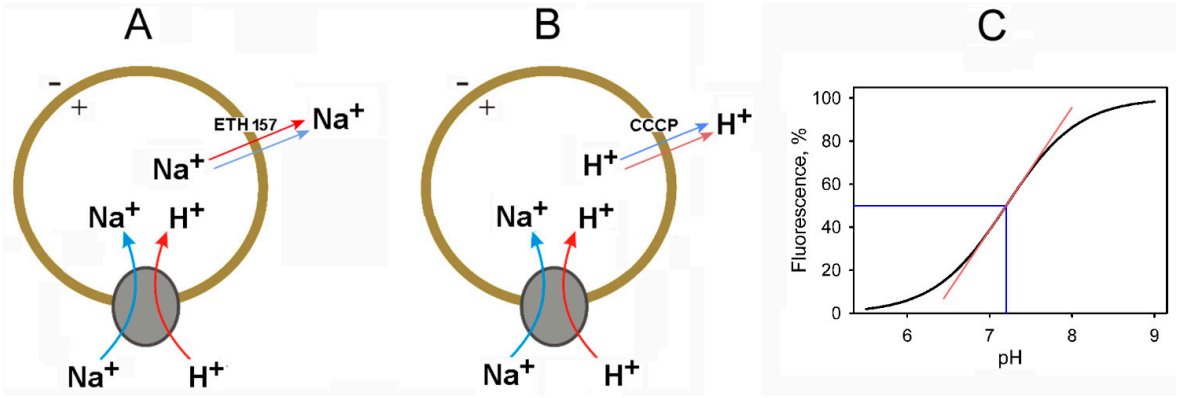

Figure 2. Measurement of H^+ and Na^+ fluxes in membrane vesicles using pyranine as a fluorescent reporter. (**A**) Ionic fluxes through the vesicle membrane (dark yellow circle) containing Na^+,H^+-PPase (gray oval) in the presence of ETH 157. Arrows of the same color refer to fluxes of the same intensity; (**B**) Same in the presence of carbonyl cyanide *m*-chlorophenylhydrazone (CCCP). The fluxes mediated by the ionophores ETH 157 or CCCP in panels (**A**,**B**) are equal to the sum of the Na^+ and H^+ fluxes through mPPase; (**C**) The theoretical pH titration curve of pyranine. The blue lines show that the pyranine fluorescence at pH equal to its pK_a of 7.2 is 50% of the maximal. The red line is the curve tangent at this point.

Similarly, pyranine fluorescence in the presence of the protonophore carbonyl cyanide *m*-chlorophenylhydrazone (CCCP) can monitor Na^+ translocation by *Bv*-mPPase with no interference from the H^+ transport [27,28]. In this setup, the H^+ ions pumped in return to the outer medium through CCCP (red arrows in Figure 2B). The protonophore also discharges the $\Delta\psi$ formed due to Na^+ pumping in by *Bv*-mPPase. In a medium lacking membrane-permeable ions other than H^+, the rate of proton release from membrane vesicles will equal the rate of Na^+ pumping in by *Bv*-mPPase (blue arrows in Figure 2B) [29]. Accordingly, *Bv*-mPPase functioning in the presence of CCCP will *alkalinize* the vesicle lumen.

Importantly, the transport measurements reported below were performed at pH 7.2, which is equal to pyranine pK_a [25], and the vesicles contained large amounts (100 mM) of a Mops buffer with the same pK_a. With this experimental setup, equal fluxes of H^+ and Na^+ ions into the vesicles should result in symmetrical fluorescence changes caused by alkalinization in the presence of CCCP or acidification in the presence of ETH 157 (Figure 2C). This evident prediction was confirmed in trial titrations of a pyranine-loaded vesicle suspension with alkali or acid in the presence of 2 μg/mL nonspecific ionophore gramicidin D. The sensitivity of the assay is determined by the slope of the tangent to the pyranine titration curve, dF/dpH, and is maximal at pH = pyranine pK_a (Figure 2C). Although this assay does not yield absolute transport rates, it allows the comparison of the Na^+- and H^+-translocating activities of Na^+,H^+-PPase under identical conditions in the same vesicle preparation.

The validity of the proposed approach was tested with the H^+-translocating mPPase of *Desulfitobacterium hafniense* (*Dh*-mPPase) and Na^+-translocating mPPase of *Desulfuromonas acetoxidans* (*Da*-mPPase) produced in *E. coli* cells. In the presence of 10 mM Na^+, these mPPases are strictly cation-specific—*Dh*-mPPase transports only H^+, whereas *Da*-mPPase transports only Na^+ [15,30]. Notably, the membrane vesicles produced by the procedure used were predominantly inverted (>90%), as estimated from the activating effect of alamethicine on their NADH oxidase activity [31] (Table S1).

As shown in Figure 3A, the PP_i addition to *Dh*-mPPase-containing vesicles progressively decreased pyranine fluorescence, i.e., acidified the vesicle lumen. Keeping in mind that the vesicle membrane is impermeable to PP_i and that lumen acidification did not occur with the vesicles prepared from non-transformed *E. coli* cells and was completely abolished by the $Na^+(K^+)/H^+$-exchanger monensin, one can infer that the pyranine signal reports on the H^+-transporting activity of *Dh*-mPPase. This conclusion was consistent with

observations that the signal did not depend on the medium Na^+ concentration and was accelerated by the K^+ ionophore valinomycin and Na^+ ionophore ETH 157 (Figure 3A), which collapsed *Dh*-mPPase-generated $\Delta\psi$. CCCP suppressed the pyranine signal (Figure 3A) as expected, by facilitating the H^+ exit from the vesicles.

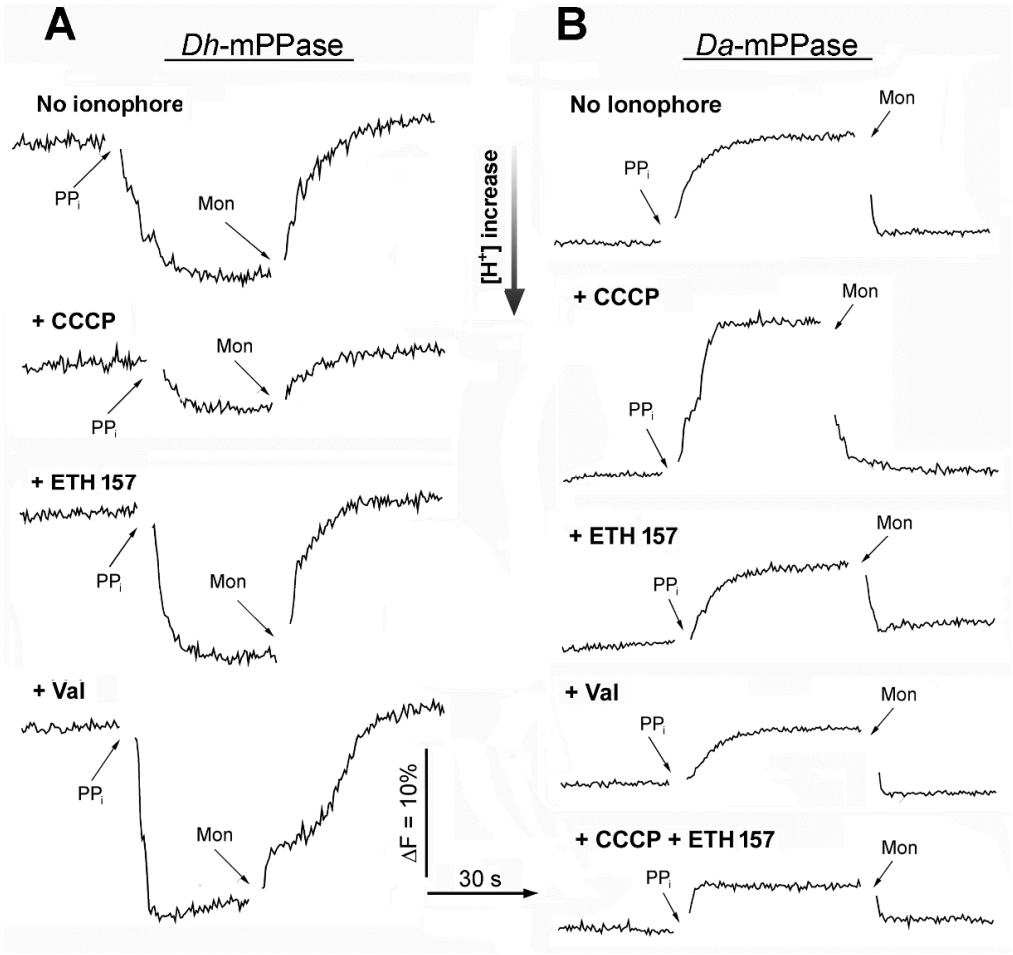

Figure 3. Entrapped pyranine fluorescence in membrane vesicles containing cation-specific mPPases. (**A**) H^+-translocating mPPase (*Dh*-mPPase); (**B**) Na^+-translocating mPPase (*Da*-mPPase). The reaction medium contained 100 mM Mops-KOH (pH 7.2), 25 mM K_2SO_4, 5 mM $MgSO_4$, 5 mM Na_2SO_4, 75 μg protein/mL membrane vesicles, and, where indicated by labels, 10 μM CCCP, 1 μM valinomycin (Val), or 20 μM ETH 157. The following components were added at the time points marked by arrows: PP_i (150 μM), monensin (Mon, 2.5 μM).

In contrast, the Na^+-translocating *Da*-mPPase caused monensin-sensitive alkalinization of the vesicle lumen in response to PP_i addition (Figure 3B) because the Na^+ accumulation stimulated passive H^+ leakage from the vesicles. CCCP increased the rate of fluorescence change by increasing the membrane permeability to protons. The rate increased monotonically with the Na^+ concentration in the range of 0.05–50 mM. The Na^+ ionophore ETH 157 and K^+ ionophore valinomycin suppressed the pyranine signal appreciably (Figure 3B) by allowing $\Delta\psi$-driven Na^+ or K^+ ions to exit from the vesicles instead of proton. The evident corollary is that the proposed transport assay adequately measures the Na^+- and H^+-translocating activities of the monospecific H^+- and Na^+-PPases.

2.2. Na^+ and H^+ Fluxes Mediated by Dual-Specificity *Bv*-mPPase

PP_i addition to the membrane vesicle harboring the promiscuous Na^+,H^+-translocating *Bv*-mPPase caused monensin-sensitive alkalinization of the vesicle lumen in the medium containing 10 mM Na^+ and no ionophores (Figure 4). Lumen alkalinization was markedly

accelerated by CCCP, indicating low membrane permeability to protons in the absence of a protonophore. The pyranine response was only partially decelerated by valinomycin, which collapsed the $\Delta\psi$. These findings were the first to indicate a marked prevalence of the Na^+-translocating activity of *Bv*-mPPase over its H^+-translocating activity—zero signal would be observed if the activities were equal. When added together, the ionophores ETH 157 and CCCP markedly suppressed lumen alkalinization (Figure 4). Notably, H^+-translocation by *Bv*-mPPase (fluorescence decrease) was detected only in the presence of ETH 157, which neglected the contribution of the Na^+-translocating activity to the pyranine signal (Figure 2A). But even in this case, the acidification of the vesicle lumen proceeded markedly slower than its alkalinization in the presence of CCCP (Figure 4). Clearly, the simultaneous fluxes of Na^+ and H^+ mediated by *Bv*-mPPase differ markedly in intensity, with the Na^+ flux prevailing.

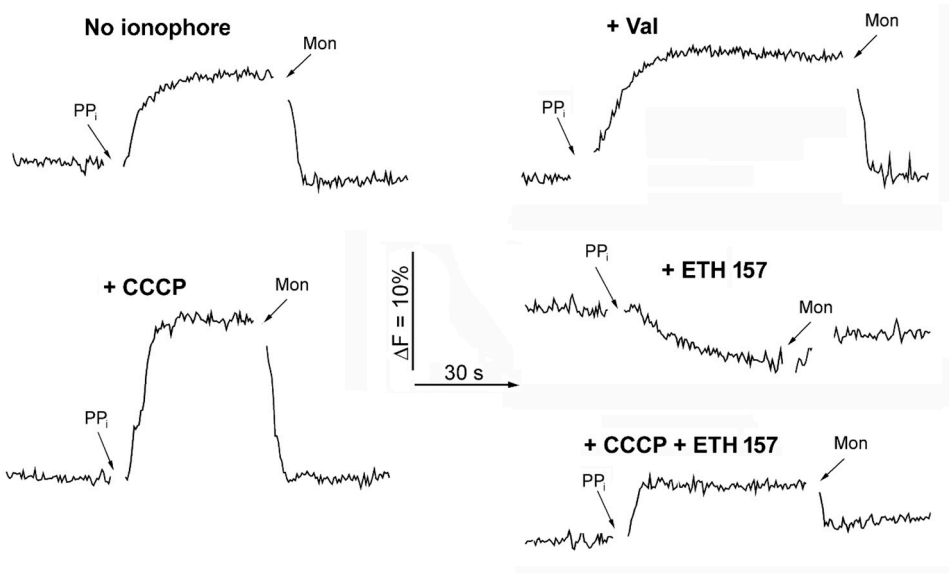

Figure 4. Entrapped pyranine fluorescence in membrane vesicles containing *B. vulgatus* Na^+,H^+-translocating mPPase. The starting reaction medium and ionophore additions to it were as shown in Figure 3.

To probe the direct effects of the ionophores on the *Bv*-mPPase, the time-courses of the P_i formation from 150 μM PP_i by *Bv*-mPPase-containing vesicles were obtained using a continuous P_i analyzer [32]. The effects of ETH 157 and valinomycin under the conditions shown in Figure 4 were insignificant (<5%) and CCCP stimulated the hydrolysis reaction by only 20% (Figure S1). These findings rule out the direct interaction of the ionophores with *Bv*-mPPase as the only explanation of their effects on the cation transport.

2.3. Fast Kinetics of Cation Transport by Bv-mPPase: Effects of Na^+ Concentration

Quantitative estimates of the initial rates of the cation transport by *Bv*-mPPase could not be obtained with precision from the data presented in Figure 4, which were measured using manual mixing. Therefore, Na^+ and H^+ transport measurements in the presence of CCCP and ETH 157, similar to those in Figure 4, were performed using a stopped-flow instrument with a mixing time of 1.6-ms. Figure 5 shows typical recordings obtained at three Na^+ concentrations. Signals corresponding to either the Na^+ or H^+-translocation were observed over the entire range of the Na^+ concentrations, consistent with earlier findings [18]. The smaller signal amplitudes than in Figure 4 are explained by the higher contribution of the light scattered by the membrane vesicles to the signal because of the inferior performance of the filter used to cut off the exciting light in the stopped-flow instrument compared with the monochromator in the conventional spectrofluorometer.

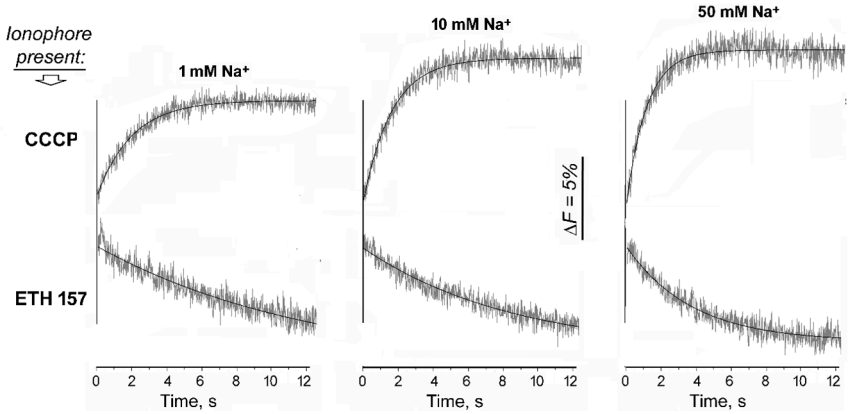

Figure 5. Stopped-flow traces of pyranine fluorescence recorded after adding PP_i to the membrane vesicles harboring *B. vulgatus* Na^+,H^+-translocating mPPase at the indicated Na^+ concentrations. Vesicle suspension [0.15 mg protein/mL, 100 mM Mops-KOH, pH 7.2, 25 mM K_2SO_4, 5 mM $MgSO_4$, different concentrations of Na^+ (added as Na_2SO_4), and 20 μM CCCP or 40 μM ETH 157, as indicated] was preincubated for 10 min and mixed with an equal volume of 300 μM PP_i solution in the same medium but without the vesicles and ionophores.

The time courses of the pyranine fluorescence in Figure 5 could be reasonably well described by a one-exponent Equation (1) or (2) (see Section 4), yielding, in each case, the absolute value of the initial velocity of the fluorescence change (v_0, a measure of the transport rate) and the conditional rate constant k (Table S2). The latter parameter does not have a physical meaning and is used only as a means to fit the data and determine the v_0 value. The Na^+-translocating activity measured with the CCCP (v_0^{Na}) and H^+-translocating activity measured with ETH 157 (v_0^{H}) increased approximately in parallel with the increase in [Na^+] (Figure 6A). However, the major finding was that the ratio v_0^{H}/v_0^{Na} was markedly less than unity and nearly constant in the 1–50 mM Na^+ concentration range (Figure 6B). Based on the v_0^{H}/v_0^{Na} values obtained (Table S2 and Figure 6B), H^+ influx contributes only ~1/8th to the total monovalent cation influx catalyzed by *Bv*-mPPase in the Na^+ concentration range tested.

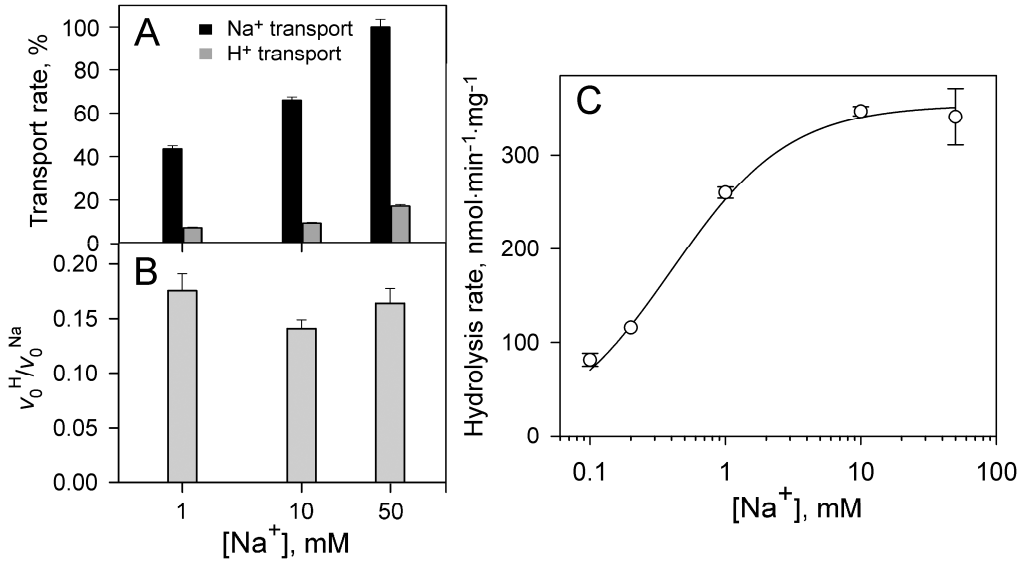

Figure 6. The dependence of the hydrolytic and transport activities of *Bv*-mPPase on Na^+ concentration. The assay medium contained 100 mM Mops-KOH (pH 7.2), 25 mM K_2SO_4, 5 mM $MgSO_4$, 150 μM PP_i, the indicated amounts of Na^+ (added as Na_2SO_4), and the membrane vesicles (2–8 and

150 μg protein/mL in the hydrolysis and transport assays, respectively). (**A**) Rates of cation transport at 1-, 10-, and 50-mM Na^+ concentrations, as calculated from the data in Figure 5 and compiled in Table S2. The Na^+ transport rate measured at 50 mM Na^+ was taken as 100%, and all other transport rates are given relative to it. Bars refer to the standard error in the fitted value of v_0 obtained from approximately 20 averaged individual time courses; (**B**) The ratio of the H^+ and Na^+ transport rates in panel (**B**); (**C**) Rates of PP_i hydrolysis. The reaction was started by adding 150 μM PP_i to an otherwise complete reaction mixture. The abscissa is logarithmically scaled. The line shows the best fit of a simple hyperbola (Michaelis–Menten-type equation) to the hydrolysis rate profile.

Notably, the Na^+ dependence of the hydrolytic activity (Figure 6C) differed from the dependences of both transport activities (Figure 6A). The former dependence was a simple hyperbola, consistent with a single essential Na^+-binding site with K_d of 0.40 ± 0.05 mM (earlier reported as 0.57 mM [18] under similar conditions), nearly saturated at 10 mM Na^+. In contrast, the transport activities required higher Na^+ concentrations for saturation (Figure 6A), suggesting a requirement for an additional, lower-affinity Na^+-binding site.

The lower absolute rate of the fluorescence change due to the H^+ transport (ETH 157 present) compared with the Na^+ transport (CCCP present) in Figures 4–6 might have resulted from the kinetic limitation of the ETH 157-mediated Na^+ efflux. Notably, the standard ETH 157 concentration used (20 μM) is near the solubility limit and could not be further increased. However, several lines of evidence ruled out the possibility of H^+ transport rate limitation by the Na^+ efflux through ETH 157. First, adding 1 μM valinomycin to the assay medium with ETH 157 to allow K^+ efflux and decrease the burden of ETH 157 did not accelerate the initial rate of fluorescence change (H^+ transport) at the 10 mM Na^+ concentration. Second, a twofold decrease in the ETH 157 concentration resulted in only a 20% decrease in $v_0{}^H$ at a 10 mM Na^+ concentration, suggesting that the 20 μM ETH concentration was nearly saturating. Finally, a higher rate of ETH 157-stimulated transport observed for the different mPPase in Figure 3A also makes it unlikely that the transportation capacity of ETH 157 was exhausted in Figures 4 and 5.

2.4. Fast Kinetics of Cation Transport by Bv-mPPase: Effects of Substrate Concentration

The preceding hydrolysis and transport measurements were conducted at a constant 150 μM PP_i concentration. Figure 7 details the effects of substrate concentration on hydrolysis and transport rates. Because mPPase activities depend on the concentration of the Mg^{2+} cofactor, its free concentration in the medium was maintained at a constant level of 4.8 mM in these experiments by taking into account its complexation with PP_i (see Section 4).

The hydrolysis rate profile shown in Figure 7A was similar to that measured earlier under similar conditions [30]. The profile is of an asymmetrical bell type—its rising and descending parts correspond to substrate binding to the first and second catalytic sites in the mPPase dimer (Scheme 1) [22,30,33,34].

Fitting Equation (3) (see Section 4) to the rate dependence in Figure 7A yielded the values for the corresponding macroscopic Michaelis constants (K_{m1} and K_{m2}) and the maximal activities of the mono- and di-substrate complexes (A_1 and A_2) listed in Table 1. Notably, the A_1 and A_2 values refer to one and two functioning active sites in dimer, respectively; hence, the actual average performance of each of the two active sites in SES was approximately one third of that of the productive subunit in ES. The macroscopic K_{m1} value previously measured for *Bv*-mPPase under similar conditions was 12 ± 1 μM in terms of the Mg_2PP_i complex [30] (corresponding to 18 μM in terms of the total PP_i, as used in this work). Figure 7B shows the distribution of the enzyme between the two enzyme–substrate complexes at different substrate concentrations, as calculated based on the K_m values obtained in this work.

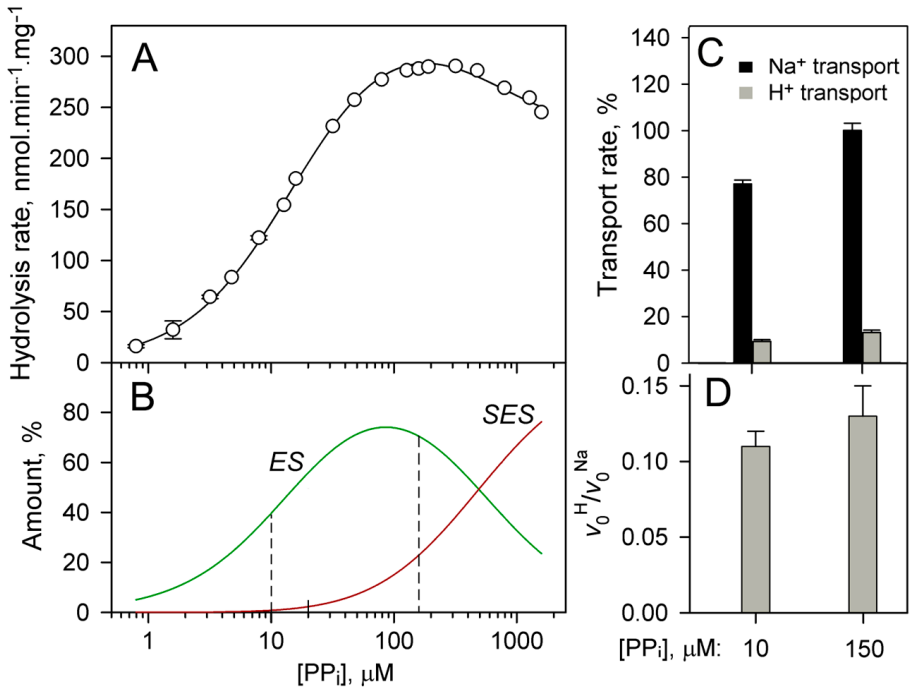

Figure 7. Dependence of the hydrolytic and transport activities of *By*-passes on PP_i concentration. The assay medium contained 100 mM Mops-KOH (pH 7.2), 25 mM K_2SO_4, 5 mM Na_2SO_4, 4.8–7.4 mM $MgSO_4$, and the membrane vesicles (2–8 and 150 μg protein/mL in the hydrolysis and transport assays, respectively). (**A**) Rates of PP_i hydrolysis. The reaction was started by adding the indicated amounts of PP_i to the otherwise complete reaction mixture. The line shows the best fit of Equation (3) to the rate profile; (**B**) Distribution of the *Bv*-mPPase dimer species with partially occupied (ES), and fully occupied (SES) catalytic sites as a function of substrate concentration. The distribution was calculated for Scheme 1 using the K_{m1} and K_{m2} values of 15 and 500 μM, respectively, as derived from the hydrolysis rate profile in panel (**A**). The dashed lines mark the amounts of ES and SES at the PP_i concentrations used in the transport assays; (**C**) Rates of cation transport at two PP_i concentrations, as estimated from the stopped-flow data in Figure 5 and Figure S2 and compiled in Table S2. The Na^+ transport rate measured at 150 μM PP_i was taken as 100%, and all other transport rates are given relative to it; (**D**) The ratio of the H^+ and Na^+ transport rates in panel (**C**).

$$\mathbf{E} \underset{}{\overset{K_{m1}}{\leftrightarrows}} \mathbf{ES} \overset{A_1 \nearrow}{\underset{}{\overset{K_{m2}}{\leftrightarrows}}} \mathbf{SES} \overset{A_2}{\rightarrow}$$

Scheme 1. Substrate binding and hydrolysis at two active sites of dimeric *Bv*-mPPase.

Table 1. Kinetic parameters for *Bv*-mPPase-catalyzed PPi hydrolysis (Scheme 1).

Parameter and Unit	Value ± SE
A_1 (nmol·min^{-1}·mg^{-1})	340 ± 10
A_2 (nmol·min^{-1}·mg^{-1})	220 ± 20
K_{m1} (μM)	15 ± 1
K_{m2} (μM)	500 ± 300

Stopped-flow transport measurements were additionally performed at a 10 μM PP_i concentration (Figure S2), and the kinetic parameters were derived from the time courses as described above (Table S2). Like the effects of Na^+ on the Na^+ and H^+ transport functions of *Bv*-mPPase, the effects of PP_i were symmetrical (Figure 7C,D)—the Na^+ and H^+ transport rates changed in parallel when the PP_i concentration was varied. By comparing the effects of the PP_i concentration on the rates of hydrolysis and the Na^+/H^+ transport and the

amounts of two enzyme-substrate complexes, one can conclude that all the activities are primarily associated with the ES complex, with a lesser or no contribution of the SES complex. These data also rule out hypothetical model(s) in which a particular transport function is associated with only one of these complexes.

3. Discussion

Transport promiscuity is not uncommon among cation transporters, including those active with the sodium ion. Na^+,K^+-ATPase [35], Na^+-coupled rotary ATP synthases [36–38], and Na^+-rhodopsin [39] can transport H^+ instead of Na^+ at low pH and/or Na^+ concentrations. *Methanosarcina acetivorans* A_1A_0-ATP synthase is unique in that it is capable of generating/consuming both Na^+ and H^+ gradients under physiological conditions, suggesting no competition between the cations [40]. Notably, all ATPases use an indirect-coupling mechanism, in which the transported protons reach the pump-loading site (located in c-subunit of the rotary ATPases) from the medium. A suitable modification of this site can change its cation-binding specificity and, hence, pump specificity [41].

mPPase differs from rotary ATPases in that its H^+ transport function is based on a "direct coupling" principle—the transported proton is generated from one of the reactants, the nucleophilic water molecule. This mechanism was proposed by Lin et al. based on the structure of the H^+-transporting mPPase, which demonstrated a close contact between the active site with the bound PP_i analog and the transport channel [20]. In the mPPase structure, the water nucleophile is located at the channel entry and is coordinated by two Asp residues [20], as in aspartic proteases [42]. This coordination positions the water molecule for attack and increases its nucleophilicity, but is insufficient to convert water into a hydroxide, unlike in soluble PPases, in which the water molecule is coordinated by three divalent metal ions [43] or two such ions and Asp [44]. The Asp-only coordination results in a much lower hydrolysis efficiency of mPPases but permits proton generation from the nucleophilic water molecule in the proper place for its subsequent transport.

Strong functional evidence for the "direct coupling" mechanism is found in the data of Li et al. [45] and Shah et al. [46], who directly measured the charge flux through H^+-translocating mPPase embedded in lipid bilayer. They observed a small signal due to the binding of the nonhydrolyzable PP_i analog imidodiphosphate, which they interpreted as a binding-induced proton transfer. They also observed a 10-fold greater signal generated by PP_i, which they ignored, perhaps because it was not recognized at that time that the latter signal resulted from a single turnover of the PP_i hydrolysis [3,47]. Simple logic tells us that if a complete turnover yields a 10-fold greater signal than the substrate binding, the latter event is not enough for a proton to cross the membrane. Clearly, substrate binding may cause a proton or other charge to cross 1/10 of the membrane thickness, but the complete translocation event (proton disappearance on one side of the membrane and appearance of the same or a different proton on its other side) requires a complete hydrolysis cycle. This seminal result unambiguously rules out substrate binding as the step at which proton translocation occurs, but nevertheless, publications from Goldman's group keep propagating this idea [22,23,48]. Notably, mPPase is the only non-oxidoreductase directly coupled proton pump—all other such pumps transport electrons [49]. Rhodopsin uses a similar mechanism to pump the proton but differs in that the transported proton appears due to a light-induced shift in retinal Schiff base pK_a, not via a chemical reaction as it is in mPPase [50].

Na^+ ion is not a reaction product and cannot be transported by mPPase in the same way as H^+. However, given the very similar architecture of Na^+- and H^+-pumping mPPases, it is highly unlikely that the "chemical" proton is not a factor in the Na^+ transport [34]. The "billiard" hypothesis described in the Introduction provided a simple way to integrate the two transport functions [3,5,47]. The hypothesis is based on structural data showing a Na^+-binding site in the ion conductance channel of the Na^+-transporting mPPase from *T. maritima* [23,45] and phylogenetic analyses showing its conservation in related mPPases. The principal Na^+ ligand at this pump-loading site is a Glu residue. Although its affinity

for protons is much greater, it is Na^+-bound under physiological conditions simply because of a much greater Na^+ concentration in comparison with the H^+ concentration. After dislodging the bound Na^+ ion into the exit channel, the "chemical" proton can occupy the Glu site and be transported in the next catalytic cycle or displaced into the cytoplasm by an incoming Na^+ ion. The choice between these possibilities depends on the Na^+ concentration, and when it is high enough, the H^+ transport should come to a stop, provided that the Na^+ binding to the Glu can completely prevent the "chemical" proton binding. This is possible if the Na^+ binding is a second-order process, whose rate tends to infinity with the increasing Na^+ concentration. Such behavior is characteristic of typical Na^+-transporting mPPases [17].

The deviation of Na^+,H^+-transporting mPPases from this rule may have several explanations. Li et al. [45] and Strauss et al. [22] proposed that Na^+ and H^+ are alternately transported by Na^+,H^+-PPase subunits, which flip between different ion gate configurations—it corresponds to H^+-PPase in one subunit, and to Na^+-PPase in the other. They also hypothesized that the transported cation binding to subunit B is necessary for product release from subunit A. However, this mechanism suggests equal rates of Na^+ and H^+ transport and is therefore inconsistent with our data.

A more likely alternative is that both transport events occur in the same subunit and the well-documented non-equivalence of subunits [22,23,30,33,51] has a different explanation. For instance, subunit A may perform hydrolysis and transport while subunit B transiently stores conformational energy, or subunits work alternately—PP_i binding to subunit B is necessary for product release from subunit A [3].

To our knowledge, the transport stoichiometry of the Na^+,H^+-PPase may have three explanations. One possibility (Model A) is that Na^+ binding to the pump-loading site involves two steps: transient binding to an auxiliary site (step 1, a second-order reaction with the rate increasing with the Na^+ concentration) followed by the Na^+ transfer to the destination (step 2, a first-order reaction with the rate independent of the Na^+ concentration). The overall binding rate then increases with the increasing Na^+ concentration to a constant level equal to the rate of step 2. In this working model, the limiting distribution of the Glu residue between H^+-bound and Na^+-bound forms at high Na^+ concentrations is determined by the relative rates of Na^+ delivery from the auxiliary site (step 2) and H^+ delivery from the transition state complex. Accordingly, a constant ratio of the H^+ and Na^+ transport rates is expected at high Na^+ concentrations. In principle, this ratio may be smaller or greater than one, and our data (Figure 6) show that it is approximately 0.14 for the *Bv*-mPPase.

That this ratio tends to zero in Na^+-transporting mPPases suggests that they lack a transitory site or that it delivers Na^+ to the pump-loading site at a much higher rate compared with H^+. The available data do not allow a rigorous choice between these alternatives. Although the published crystal structures of the Na^+-transporting mPPase from *T. maritima* revealed a single pump-loading Na^+-binding site per subunit [23,45], functional data indicated the presence of an additional, Na^+-specific high-affinity site, whose occupancy by Na^+ is required for PP_i hydrolysis and H^+/Na^+ transport [17,24,52]. Given that the crystal structure does not necessarily reveal all binding sites, the "two Na^+ sites" model is preferable, but further work is clearly needed, including a determination of the structure of Na^+,H^+-PPase in a Na^+-bound state.

Alternatively, the "chemical" proton may partially reverse Na^+ binding to the pump-loading site, which becomes a bifurcation point in the Na^+ pathway in this case (Model B). In other words, there may be a non-zero probability that the released "chemical" proton directs a fraction of bound Na^+ ions back to the cytoplasm or an alternative location and partially occupies the pump-loading site. In this case, the H^+/Na^+ transport ratio may also decrease to a constant level with the increasing Na^+ concentration.

Models A and B imply the transport stoichiometry of approximately 0.9 Na^+ and 0.1 H^+ ion, summing up to 1 ion per each hydrolyzed PP_i molecule. Because our data estimate only the ratio of transport rates, they permit the stoichiometry of 1 Na^+ and

0.11 H^+ ions per PP_i molecule hydrolyzed, giving more than one cation in total. This could happen if the "chemical" proton could enter the exit channel together with Na^+ in a fraction of catalytic cycles, provided that the time during which the channel is open permits this (Model C). In Model C, the transportations of Na^+ and H^+ are thus intrinsically coupled in the catalytic cycle, whereas they are competing processes in Models A and B. The independence of the H^+/Na^+ transport ratio on the Na^+ concentration in Model C may have the same explanation as in Model A or B.

To summarize, the results reported above provide functional and kinetic insights into the ion transport mechanisms underlying the dual transport specificity of pyrophosphate-driven Na^+ pumps. Notably, Na^+,H^+-PPases are abundant in gut bacteria and considered to represent a means of adapting to environmental challenges (anaerobiosis and intense niche competition) [18]. Further work is clearly required to reliably choose between the transport and hydrolysis models mentioned above and to delineate the general transport mechanism in sufficient detail to explain the transport promiscuity of mPPases. This work will likely involve site-directed mutagenesis along with the aforementioned assays and time-resolved structural studies using direct methods and molecular dynamics simulations.

4. Materials and Methods

4.1. Materials

Pyranine was obtained from Eastman Kodak (Rochester, NY, USA); Tris (Trizma base), valinomycin, and carbonyl cyanide *m*-chlorophenylhydrazone (CCCP) were obtained from Sigma-Aldrich Co (St. Lous, MO, USA); Mops was an Amresco (Solon, OH, USA) product; the Na^+ ionophore ETH 157 and K_2SO_4 were from Fluka Chemie (Buchs, Switzerland); magnesium sulfate hexahydrate was from Merck (Rahway, NJ, USA); disodium sulfate was from Reachim (Moscow, Russia); monensin was obtained from Serva-Feinbiochemica (Heidelberg, Germany).

4.2. Production of mPPases in Escherichia coli and Isolation of Membrane Vesicles

Plasmids with genes for mPPases from *B. vulgatus* (*Bv*-mPPase) [17], *Desulfitobacterium hafniense* (*Dh*-mPPase) [30], and *Desulfuromonas acetoxidans* (*Da*-mPPase) [15] were expressed in *E. coli* C41(DE3) cells as described elsewhere [30]. *E. coli* cells were harvested via centrifugation (10,000× *g*, 10 min) and washed with medium containing 85 mM NaCl, 5 mM $MgSO_4$, and 10 mM Tris-HCl, pH 7.5. The sediment was suspended in medium A (100 mM Mops-KOH, pH 7.2, 25 mM K_2SO_4, 5 mM $MgSO_4$) containing 1 mM pyranine and traces of DNase. The mixture was passed once through a French press at 16,000 psi, the unbroken cells and cell debris were removed by centrifugation at 27,500× *g* (5 min), and membrane vesicles were sedimented at 150,000× *g* (50 min). The vesicles were additionally washed with medium A via two cycles of resuspension/centrifugation (150,000× *g*, 40 min) and immediately used for transport and hydrolytic activity measurements. Vesicles were quantitated in terms of their protein concentration using a bicinchoninic acid method [53] with bovine serum albumin as a standard. mPPase activities of the membrane vesicles harboring *Bv*-mPPase, *Dh*-mPPase, or *Da*-mPPase were 0.34, 1.2, and 0.60 μmol·min^{-1}·mg protein^{-1}, respectively. Sodium fluoride (1 mM) was added to the activity assay to inhibit traces of contaminating *E. coli* cytosolic PPase.

4.3. Assay of the Hydrolytic Activity

The rates of PP_i hydrolysis were measured at 25 °C using a continuous P_i assay [32] with a sensitivity of 6 μM P_i per recorder scale. The reaction mixture of 20 mL volume typically contained 100 mM Mops-KOH buffer, pH 7.2, 5 mM $MgSO_4$, 25 mM K_2SO_4, 5 mM Na_2SO_4, and membrane vesicles (2–16 μg protein/mL). The reaction was started by the addition of 150 μM PP_i (tetrasodium salt), and P_i liberation was monitored for 3–4 min. Variations in the assay composition are specified in figure legends. All activity measurements were performed in duplicate, and appropriate corrections were made for PP_i

interference with P_i assay [33]. Hydrolysis rates (mPPase activities) are presented below in terms of the molar amount of PP_i hydrolyzed per 1 min per 1 mg of vesicle protein.

4.4. Assay of the Transport Activities

The acidification and alkalinization of the vesicle interior were monitored by measuring the fluorescence of the entrapped pyranine at 510 nm with excitation at 458 nm in medium A containing different concentrations of Na_2SO_4. The contaminating Na^+ concentration in medium A was approximately 50 μM, as measured using a flame photometer (UNICO-SYS, Saint Petersburg, Russia). Fluorescence measurements were performed using a FluoroMax-3 spectrofluorometer (Horiba Jobin Yvon, Stow, MA, USA). The vesicles were preincubated for 5 min in the assay medium before adding 150 μM PP_i (tetrapotassium salt). Other additions to the assay medium are described in the figure legends. PP_i and monensin were added from their respective 100 mM and 2.5 mM stock solutions.

Stopped-flow measurements of the fluorescence time courses upon PP_i addition to the membrane vesicles containing entrapped pyranine were performed on a rapid kinetics apparatus (BioLogic Science Instruments, Seyssinet-Pariset, France) consisting of an SFM-3000/S stopped-flow mixer and MOS-200 optical system with a 3-μL cuvette. The excitation wavelength was set at 458 nm (monochromator slit width of 4 nm) and emission was detected at >495 nm using a SCHOTT GG495 filter (Mainz, Germany). Equal volumes (13 μL each) of the vesicle suspension and PP_i solution in the same buffer were mixed at 25 °C at a flow rate of 1.2 mL/s (dead-time of 1.6 ms), and fluorescence was monitored for 20 s at a 10-ms resolution. Data from approximately 20 shots were averaged in each case.

4.5. Data Treatment

All nonlinear least-squares data fittings were performed using Scientist software version 2.01 (MicroMath, Salt Lake City, UT, USA). Stopped-flow data were analyzed in terms of simple first-order kinetics using Equation (1) (fluorescence rise) or 2 (fluorescence decay), where F is the fluorescence, v_0 is the initial rate of fluorescence change, k is the rate constant, t is time, and a is F offset; the ratio v_0/k is equal to the amplitude of the signal change.

$$F = a + (v_0/k)\cdot[1 - \exp(-kt)] \quad (1)$$

$$F = a + (v_0/k)\cdot \exp\,(-kt) \quad (2)$$

Cooperative kinetics of PP_i hydrolysis was analyzed in terms of Scheme 1 [30], where K_{m1} and K_{m2} are the Michaelis constants for consecutive PP_i (S) binding to two active sites in the enzyme dimer (E); A_1 and A_2 are the specific rates for the ES, and SES species, respectively. The corresponding rate equation (Equation (3)) implies steady-state kinetics for substrate binding and conversion. The scheme and equation(s) describe hydrolysis kinetics in terms of macroscopic Michaelis constants, i.e., do not distinguish between the two ES species containing substrate in different subunits of the dimer.

$$v = (A_1 + A_2[S]/K_{m2})/(1 + K_{m1}/[S] + [S]/K_{m2}) \quad (3)$$

All kinetic measurement reported above were performed at a free Mg^{2+} concentration of 4.8 mM in the reaction media. To accomplish this, we calculated the amounts of the Mg^{2+} ions bound in $MgPP_i$ and Mg_2PP_i complexes formed at each PP_i concentration using the published data on the equilibria in the Mg^{2+}–PP_i system [32] and increased the amount of the added magnesium salt appropriately. In the presence of 4.8 mM Mg^{2+} ions, 63% of the total PP_i exist as the Mg_2PP_i complex, the presumed true substrate of mPPase, at pH 7.2 [32].

Supplementary Materials: The supporting information can be downloaded at: https://www.mdpi.com/article/10.3390/ijms252211963/s1.

Author Contributions: Conceptualization, A.V.B.; methodology, A.V.B., V.A.A. and E.G.Z.; validation, all authors; formal analysis, A.V.B. and V.A.A.; investigation, A.V.B., V.A.A. and Y.V.B.; resources, A.V.B., V.A.A. and E.G.Z.; writing—original draft preparation, A.V.B. and A.A.B.; writing—review and editing, all authors.; visualization, A.V.B. and A.A.B.; supervision, A.V.B. and A.A.B.; funding acquisition, A.A.B. All authors have read and agreed to the published version of the manuscript.

Funding: This work was funded by the Russian Science Foundation (research project 23-24-00115).

Institutional Review Board Statement: Not applicable.

Informed Consent Statement: Not applicable.

Data Availability Statement: The data presented in this study are available on request from the authors.

Acknowledgments: The stopped-flow apparatus used in this work is part of the MSU Shared Research Equipment Center 'Subdiffractional Microscopy and Spectroscopy' and was purchased in the framework of the Equipment Renovation Program of the National Project 'Science'.

Conflicts of Interest: The authors declare no conflicts of interest.

References

1. Baltscheffsky, H.; von Stedingk, L.V.; Heldt, H.W.; Klingenberg, M. Inorganic pyrophosphate: Formation in bacterial photophosphorylation. *Science* **1966**, *153*, 1120–1122. [CrossRef] [PubMed]
2. Baltscheffsky, M. Inorganic pyrophosphate and ATP as energy donors in chromatophores from *Rhodospirillum rubrum*. *Nature* **1967**, *216*, 241–243. [CrossRef] [PubMed]
3. Baykov, A.A.; Anashkin, V.A.; Malinen, A.M.; Bogachev, A.V. The mechanism of energy coupling in H^+/Na^+-pumping membrane pyrophosphatase—Possibilities and probabilities. *Int. J. Mol. Sci.* **2022**, *23*, 9504. [CrossRef] [PubMed]
4. Tsai, J.-Y.; Kellosalo, J.; Sun, Y.-J.; Goldman, A. Proton/sodium pumping pyrophosphatases: The last of the primary ion pumps. *Curr. Opin. Struct. Biol.* **2014**, *27*, 38–47. [CrossRef]
5. Baykov, A.A.; Malinen, A.M.; Luoto, H.H.; Lahti, R. Pyrophosphate-fueled Na^+ and H^+ transport in prokaryotes. *Microbiol. Mol. Biol. Rev.* **2013**, *77*, 267–276. [CrossRef]
6. Serrano, A.; Pérez-Castiñeira, J.R.; Baltscheffsky, M.; Baltscheffsky, H. H^+-PPases: Yesterday, today and tomorrow. *IUBMB Life* **2007**, *59*, 76–83. [CrossRef]
7. García-Contreras, R.; de la Mora, J.; Mora-Montes, H.M.; Martínez-Álvarez, J.A.; Vicente-Gómez, M.; Padilla-Vaca, F.; Vargas-Maya, N.I.; Franco, B. The inorganic pyrophosphatases of microorganisms: A structural and functional review. *Peer J.* **2024**, *12*, 17496. [CrossRef]
8. Maeshima, M. Vacuolar H^+ -pyrophosphatase. *Biochim. Biophys. Acta Biomembr.* **2000**, *1465*, 37–51. [CrossRef]
9. Lander, N.; Cordeiro, C.; Huang, G.; Docampo, R. Polyphosphate and acidocalcisomes. *Biochem. Soc. Trans.* **2016**, *44*, 1–6. [CrossRef]
10. Heinonen, J.K. *Biological Role of Inorganic Pyrophosphate*; Kluwer Academic Publishers: London, UK, 2001; pp. 77–78.
11. Gaxiola, R.A.; Palmgren, M.G.; Schumacher, K. Plant proton pumps. *FEBS Lett.* **2007**, *581*, 2204–2214. [CrossRef]
12. Martinoia, E.; Maeshima, M.; Neuhaus, H.E. Vacuolar transporters and their essential role in plant metabolism. *J. Exp. Bot.* **2007**, *58*, 83–102. [CrossRef] [PubMed]
13. Malykh, E.A.; Golubeva, L.I.; Kovaleva, E.S.; Shupletsov, M.S.; Rodina, E.V.; Mashko, S.V.; Stoynova, N.V. H^+-translocating membrane-bound pyrophosphatase from *Rhodospirillum rubrum* fuels *Escherichia coli* cells via an alternative pathway for energy generation. *Microorganisms* **2023**, *11*, 294. [CrossRef]
14. Sreenivas, K.; Eisentraut, L.; Brink, D.P.; Persson, V.C.; Carlquist, M.; Gorwa-Grauslund, M.F.; van Niel, E.W.J. Evaluation of pyrophosphate-driven proton pumps in *Saccharomyces cerevisiae* under stress conditions. *Microorganisms* **2024**, *12*, 625. [CrossRef] [PubMed]
15. Luoto, H.; Belogurov, G.A.; Baykov, A.A.; Lahti, R.; Malinen, A.M. Na^+-translocating membrane pyrophosphatases are widespread in the microbial world and evolutionarily precede H^+-translocating pyrophosphatases. *J. Biol. Chem.* **2011**, *286*, 21633–21642. [CrossRef]
16. Biegel, E.; Müller, V.A. A Na^+-translocating pyrophosphatase in the acetogenic bacterium *Acetobacterium woodie*. *J. Biol. Chem.* **2011**, *286*, 6080–6084. [CrossRef] [PubMed]
17. Luoto, H.H.; Nordbo, E.; Baykov, A.A.; Lahti, R.; Malinen, A.M. Membrane Na^+-pyrophosphatases can transport protons at low sodium concentrations. *J. Biol. Chem.* **2013**, *288*, 35489–35499. [CrossRef]
18. Luoto, H.H.; Baykov, A.A.; Lahti, R.; Malinen, A.M. Membrane-integral pyrophosphatase subfamily capable of translocating both Na^+ and H^+. *Proc. Natl. Acad. Sci. USA* **2013**, *110*, 1255–1260. [CrossRef]
19. Nordbo, E.; Luoto, H.H.; Baykov, A.A.; Lahti, R.; Malinen, A.M. Two independent evolutionary routes to Na^+/H^+ cotransport function in membrane pyrophosphatases. *Biochem. J.* **2016**, *473*, 3099–3111. [CrossRef]

20. Lin, S.M.; Tsai, J.Y.; Hsiao, C.D.; Huang, C.Y.; Chiu, T.L.; Liu, M.H.; Tung, J.Y.; Liu, T.H.; Pan, R.L.; Sun, Y.J. Crystal structure of a membrane-embedded H^+-translocating pyrophosphatase. *Nature* **2012**, *484*, 399–403. [CrossRef]
21. Kellosalo, J.; Kajander, T.; Kogan, K.; Pokharel, K.; Goldman, A. The structure and catalytic cycle of a sodium-pumping pyrophosphatase. *Science* **2012**, *337*, 473–476. [CrossRef]
22. Strauss, J.; Wilkinson, C.; Vidilaseris, K.; de Castro Ribeiro, O.M.; Liu, J.; Hillier, J.; Wichert, M.; Malinen, A.M.; Gehl, B.; Jeuken, L.J.S.; et al. Functional and structural asymmetry suggest a unifying principle for catalysis in membrane-bound pyrophosphatases. *EMBO Rep.* **2023**, *25*, 853–875. [CrossRef] [PubMed]
23. Vidilaseris, K.; Kiriazis, A.; Turku, A.; Khattab, A.; Johansson, N.G.; Leino, T.O.; Kiuru, P.S.; Boije af Gennäs, G.; Meri, S.; Yli-Kauhaluoma, J.; et al. Asymmetry in catalysis by *Thermotoga maritima* membrane bound pyrophosphatase demonstrated by a nonphosphorus allosteric inhibitor. *Sci. Adv.* **2019**, *5*, eaav7574. [CrossRef] [PubMed]
24. Kano, K.; Fendler, J.H. Pyranine as a sensitive pH probe for liposome interiors and surfaces. pH gradients across phospholipid vesicles. *Biochim. Biophys. Acta* **1978**, *509*, 289–299. [CrossRef] [PubMed]
25. Clement, N.R.; Gould, J.M. Pyranine (8-hydroxy-1,3,6-pyrenetrisulfonate) as a probe of internal aqueous hydrogen ion concentration in phospholipid vesicles. *Biochemistry* **1981**, *20*, 1534–1538. [CrossRef]
26. Damiano, E.; Bassilana, M.; Rigaud, J.L.; Leblanc, G. Use of the pH sensitive fluorescence probe pyranine to monitor internal pH changes in *Escherichia coli* membrane vesicles. *FEBS Lett.* **1984**, *166*, 120–124. [CrossRef]
27. Zhou, W.; Bertsova, Y.V.; Feng, B.; Tsatsos, P.; Verkhovskaya, M.L.; Gennis, R.B.; Bogachev, A.V.; Barquera, B. Sequencing and preliminary characterization of the Na^+-translocating NADH:ubiquinone oxidoreductase from *Vibrio harveyi*. *Biochemistry* **1999**, *38*, 16246–16252. [CrossRef]
28. Bertsova, Y.V.; Baykov, A.A.; Bogachev, A.V. A simple strategy to differentiate between H^+- and Na^+-transporting NADH:quinone oxidoreductases. *Arch. Biochem. Biophys.* **2020**, *681*, 108266. [CrossRef]
29. Bogachev, A.V.; Murtazina, R.A.; Skulachev, V.P. The Na^+/e^- stoichiometry of the Na^+-motive NADH:quinone oxidoreductase in *Vibrio alginolyticus*. *FEBS Lett.* **1997**, *409*, 475–477. [CrossRef]
30. Artukka, E.; Luoto, H.H.; Baykov, A.A.; Lahti, R.; Malinen, A.M. Role of the potassium/lysine cationic center in catalysis and functional asymmetry in membrane-bound pyrophosphatases. *Biochem. J.* **2018**, *475*, 1141–1158. [CrossRef]
31. Bertsova, Y.V.; Bogachev, A.V. Operation of the cbb_3-type terminal oxidase in *Azotobacter vinelandii*. *Biochemistry* **2002**, *67*, 622–626.
32. Baykov, A.A.; Anashkin, V.A.; Malinen, A.M. Good-practice non-radioactive assays of inorganic pyrophosphatase activities. *Molecules* **2021**, *26*, 2356. [CrossRef] [PubMed]
33. Anashkin, V.A.; Malinen, A.M.; Bogachev, A.V.; Baykov, A.A. Catalytic asymmetry in homodimeric H^+-pumping membrane pyrophosphatase demonstrated by non-hydrolyzable pyrophosphate analogs. *Int. J. Mol. Sci.* **2021**, *22*, 9820. [CrossRef] [PubMed]
34. Malinen, A.M.; Anashkin, V.A.; Orlov, V.N.; Bogachev, A.V.; Lahti, R.; Baykov, A.A. Pre-steady-state kinetics and solvent isotope effects support the "billiard type" transport mechanism in Na^+-translocating pyrophosphatase. *Protein Sci.* **2022**, *31*, e4394. [CrossRef]
35. Hara, Y.; Yamada, J.; Nakao, M. Proton transport catalyzed by the sodium pump. Ouabain-sensitive ATPase activity and the phosphorylation of Na,K-ATPase in the absence of sodium ions. *J. Biochem.* **1986**, *99*, 531–539. [CrossRef]
36. Laubinger, W.; Dimroth, P. The sodium ion translocating adenosinetriphosphatase of *Propionigenium modestum* pumps protons at low sodium ion concentrations. *Biochemistry* **1989**, *28*, 7194–7198. [CrossRef]
37. Reidlinger, J.; Müller, V. Purification of ATP synthase from *Acetobacterium woodii* and identification as a Na^+-translocating F_1F_O-type enzyme. *Eur. J. Biochem.* **1994**, *223*, 275–283. [CrossRef]
38. Dimroth, P. Primary sodium ion translocating enzymes. *Biochim. Biophys. Acta* **1997**, *1318*, 11–51. [CrossRef]
39. Kato, Y.; Inoue, K.; Kandori, H. Kinetic analysis of H^+-Na^+ selectivity in a light-driven Na^+-pumping rhodopsin. *J. Phys. Chem. Lett.* **2015**, *6*, 5111–5115. [CrossRef] [PubMed]
40. Schlegel, K.; Leone, V.; Faraldo-Gómez, J.D.; Müller, V. Promiscuous archaeal ATP synthase concurrently coupled to Na^+ and H^+ translocation. *Proc. Natl. Acad. Sci. USA* **2012**, *109*, 947–952. [CrossRef]
41. Krah, A.; Pogoryelov, D.; Langer, J.D.; Bond, P.J.; Meier, T.J.; Garaldo-Gómez, D. Structural and energetic basis for H^+ versus Na^+ binding selectivity in ATP synthase F_o rotors. *Biochim. Biophys. Acta* **2010**, *1797*, 763–772. [CrossRef]
42. Meek, T.D. Catalytic mechanisms of the aspartic proteases. In *Comprehensive Biological Catalysis*; Sinnott, M., Ed.; Academic Press: San Diego, CA, USA, 1998; Volume 3, pp. 327–344.
43. Fabrichniy, I.P.; Lehtiö, L.; Tammenkoski, M.; Zyryanov, A.B.; Oksanen, E.; Baykov, A.A.; Lahti, R.; Goldman, A. A trimetal site and substrate distortion in a family II inorganic pyrophosphatase. *J. Biol. Chem.* **2007**, *282*, 1422–1431. [CrossRef] [PubMed]
44. Heikinheimo, P.; Tuominen, V.; Ahonen, A.-K.; Teplyakov, A.; Cooperman, B.S.; Baykov, A.A.; Lahti, R.; Goldman, A. Towards a quantum mechanical description of metal assisted phosphoryl transfer in pyrophosphatase. *Proc. Natl. Acad. Sci. USA* **2001**, *98*, 3121–3126. [CrossRef] [PubMed]
45. Li, K.M.; Wilkinson, C.; Kellosalo, J.; Tsai, J.Y.; Kajander, T.; Jeuken, L.J.C.; Sun, Y.J.; Goldman, A. Membrane pyrophosphatases from *Thermotoga maritima* and *Vigna radiata* suggest a conserved coupling mechanism. *Nat. Commun.* **2016**, *7*, 13596. [CrossRef] [PubMed]
46. Shah, N.R.; Wilkinson, C.; Harborne, S.P.; Turku, A.; Li, K.M.; Sun, Y.J.; Sarah Harris, S.; Goldman, A. Insights into the mechanism of membrane pyrophosphatases by combining experiment and computer simulation. *Struct. Dyn.* **2017**, *4*, 032105. [CrossRef]
47. Baykov, A.A. Energy coupling in cation-pumping pyrophosphatase—Back to Mitchell. *Front. Plant Sci.* **2020**, *11*, 107. [CrossRef]

48. Holmes, A.O.M.; Kalli, A.C.; Goldman, A. The function of membrane integral pyrophosphatases from whole organism to single molecule. *Front. Mol. Biosci.* **2019**, *6*, 132. [CrossRef]
49. Calisto, F.; Sousa, F.M.; Sena, F.V.; Refojo, P.N.; Pereira, M.M. Mechanisms of energy transduction by charge translocating membrane proteins. *Chem. Rev.* **2021**, *121*, 1804–1844. [CrossRef]
50. Ernst, O.P.; Lodowski, D.T.; Elstner, M.; Hegemann, P.; Brown, L.S.; Kandori, H. Microbial and animal rhodopsins: Structures, functions, and molecular mechanisms. *Chem. Rev.* **2014**, *114*, 126–163. [CrossRef]
51. Anashkin, V.A.; Baykov, A.A. A lumenal loop associated with catalytic asymmetry in plant vacuolar H^+-translocating pyrophosphatase. *Int. J. Mol. Sci.* **2021**, *22*, 12902. [CrossRef]
52. Belogurov, G.A.; Malinen, A.M.; Turkina, M.V.; Jalonen, U.; Rytkönen, K.; Baykov, A.A.; Lahti, R. Membrane bound pyrophosphatase of *Thermotoga maritima* requires sodium for activity. *Biochemistry* **2005**, *44*, 2088–2096. [CrossRef]
53. Smith, P.K.; Krohn, R.I.; Hermanson, G.T.; Mallia, A.K.; Gartner, F.H.; Provenzano, M.D.; Fujimoto, E.K.; Goeke, N.M.; Olson, B.J.; Klenk, D.C. Measurement of protein using bicinchoninic acid. *Anal. Biochem.* **1985**, *150*, 76–85. [CrossRef] [PubMed]